International Journal of Greenhouse Gas Control 15 (2013) 3–15

Contents lists available at SciVerse ScienceDirect

International Journal of Greenhouse Gas Control

journal homepage: www.elsevier.com/locate/ijggc

Kinetic modelling of CO_2–water–rock interactions

Helge Hellevang*, Van T.H. Pham, Per Aagaard

Department of Geosciences, University of Oslo, Pb. 1047, Blindern, Oslo, Norway

ARTICLE INFO

Article history:
Received 24 August 2012
Received in revised form 14 January 2013
Accepted 17 January 2013
Available online 28 February 2013

Keywords:
CO_2–water–rock interactions
CO_2 storage
Geochemical modelling
Analytical solution

ABSTRACT

A system perturbated by CO_2 injection reacts by dissolving primary minerals and form new secondary phases. The importance of such mineral reactions for safe long-term storage is highly system dependent, with some reservoirs rich in reactive phases that contain divalent metal cations, which promote mineral carbonte growth, and other reservoirs being almost pure quartz (SiO_2) sands. Because of the complexity in the reaction paths of natural systems, numerical simulations have proved to be valuable to predict the reactivity on time scales from laboratory experiments to tens or hundreds of thousands of years. Such numerical simulations require quality thermodynamic and kinetic data, as well as proper mathematical expressions.

We here provide a guide to model kinetically constrained CO_2–water–rock interactions aimed for both experienced geochemists and researchers with more limited background in modelling geochemical reactions. Because rates of mineral reactions are coupled through common aqueous species, and rates vary by more than ten orders of magnitude, the system of ordinary differential equations (ODE's) is commonly stiff. This leads to challenges in solving such equations and limits the possible system size and spatial and geometrical complexity that can be solved. We have here focused on how different simplifications can be made to reduce the CPU time required to solve mineral reactions and to allow reaction path modelling even for the largest scales. For a 10,000 years batch reaction simulation, we showed how the CPU run time decreased from hours when all minerals were defined by ODE's (fully kinetic), to a few seconds if secondary phases were allowed to grow according to the local equilibrium assumption (semi-kinetic). We then showed how the system can be further simplified by allowing far-from-equilibrium dissolving minerals to be expressed by first-order decay analytical expressions. We finally suggest a step-wise procedure where significant mineral reactions were first identified by running batch simulations, and the system were then simplified according to the system size, geometric complexity, and the time of interest.

© 2013 Elsevier Ltd. All rights reserved.

1. Background

Information on the thermodynamic state and the reactivity of reservoir systems are obtained through field studies, through well- and core data, laboratory experiments, thermodynamic equilibrium calculations, and more complex numerical simulations integrating kinetic equations for complex mineral assemblages. The knowledge obtained is used to predict features such as the reservoir quality of petroleum systems, the integrity of radioactive waste deposits, the long-term potential for geological storage of CO_2, and so on.

A simple and powerful way to predict the direction and extent of mineral reactions is to use the principles of equilibrium thermodynamics, where the system reacts spontaneous towards a lower total free energy. Such calculations only requires knowledge on the thermodynamic stability of minerals, organic compounds, aqueous solutes, gases and water, which are available in comprehensive thermodynamic databases such as those derived and compiled by Holland and Powell (1998), and Helgeson and coworkers (Johnson et al., 1992; Shock and Helgeson, 1990). The calculations are simple and do not require heavy computations. However, although simple thermodynamic considerations have proved to be useful in understanding natural systems (e.g., Aagaard et al., 1990), the common assumption of equilibrium between all components and phases in such systems may lead to misinterpretations. For example, mineral meta-stability and the lack of formation of phases such as quartz and dolomite at low temperatures cannot be explained within the framework of equilibrium thermodynamics alone. Related to this is the lack of a time dimension in equilibrium thermodynamics. Therefore, with the rapid increase in accessible computer power during the last decades, and with the development of a transition state theory (TST) for mineral reactions that combined equilibrium thermodynamics with rates of mineral reactions (Lasaga, 1981; Aagaard and Helgeson,

* Corresponding author. Tel.: +47 22857026.
E-mail address: helge.hellevang@geo.uio.no (H. Hellevang).

1750-5836/$ – see front matter © 2013 Elsevier Ltd. All rights reserved.
http://dx.doi.org/10.1016/j.ijggc.2013.01.027

1982), the rule today is to run kinetic simulations. Moreover, because there has been a believe that TST equations can model mineral rates at any saturation state if the far-from-equilibrium dissolution rate is known, most kinetic modelling has relied on dissolution rate data only (e.g., Xu et al., 2005; Gaus et al., 2005a; Marini, 2006). The accuracy of such numerical simulations depends partly on the rate data. Laboratory experiments have supported us with rate data for a large number of minerals at various temperatures, solute concentrations and at various distances from equilibrium. Most of these experiments have been done at far-from-equilibrium undersaturation, and TST has been used to predict growth rates from these data. There has however recently been expressed doubt on the validity of using the TST in this way to predict growth rates (e.g., Hellevang and Aagaard, 2010; Pham et al., 2011). For example, comparisons between experimental determined dolomite and magnesite growth rates and TST estimated rates, show orders of magnitude differences, and contrary to what is observed in nature, the TST approach predicts growth of these phases down to low temperatures (e.g., Pham et al., 2011). Other challenges in using laboratory data to predict the reactivity of natural systems for long time spans is the apparent difference in reactivity of laboratory and natural systems (White and Brantley, 2003), and the difficulty to define the reactive surface areas for natural systems (e.g., Lüttge, 2005).

Although recent reports have shown that the use of TST, especially on short time scales, may overestimates carbonate growth by orders of magnitude (Hellevang and Aagaard, 2010; Pham et al., 2011), it is still the preferred choice for engineering calculations due to its simplicity and due to its implementation in codes like TOUGHREACT (e.g., Xu et al., 2011). We aim to provide a scheme for simplifying the kinetic differential equations into analytical expressions to allow kinetics to be included for basin scale reactive transport simulations, after first obtaining best possible data on the system using the equations and rate parameters suggested in Pham et al. (2011). Although advective transport, diffusion and reactions are tightly connected, we here focus only on the sink or source terms in the advection–diffusion–reaction equations. We give an overview of where compilations of thermodynamic and kinetic data can be found, and present some of the key limitations in using the data for modelling CO_2 storage. To illustrate, we perform batch simulations and equilibrium thermodynamic calculations using the low-temperature Sleipner CO_2 injection into the Utsira Sand as a benchmark case. For readers interested in the coupled flow–reaction processes, a comprehensive review on the role and impact of CO_2–fluid–rock interactions in sedimentary environments have been given by Gaus (2010). Moreover, all numerical calculations in this work are done using PHREEQC, and no intercomparison of codes was done. For such a comparison we refer to Gundogan et al. (2011) who compared various codes (PHREEQC, TOUGHREACT, GEM) on CO_2–water–rock interactions.

2. On assembling data for the thermodynamic and kinetic calculations

Accurate predictions of long-term water–rock interactions require consistent thermodynamic and kinetic data. Thermodynamic data are available for a large number of minerals, gases and aqueous species in compilations such as generated for the SUPCRT92 (Johnson et al., 1992) or THERMOCALC (Holland and Powell, 1998) programs, and for geochemical simulation tools such as the PHREEQC v2 program (Parkhurst and Appelo, 1999). For example, the commonly used 'llnl.dat' file provided with the PHREEQC program contains stability data and required speciation data for more than 1100 phases (minerals, gases, solvents). A common challenge is that mineral phases of interest lack in the database (Gaus et al., 2008). Many of the missing minerals are so called solid-solutions, and have compositions and thermodynamic properties that reflect a mixture of two or more end-members. Most clay minerals (e.g., chlorites) and some carbonate that are likely to form during CO_2 storage (e.g., ankerite ($CaFe_{0.6}Mg_{0.4}(CO_3)_2$), are examples of such solid-solutions. There are several approaches to estimate the thermodynamic values for solid-solution minerals (e.g., Aagaard and Helgeson, 1983; Powell and Holland, 1999). If minerals lack in the database, the solution is commonly either to use proxy minerals, or to incorporate or estimate thermodynamic data from other sources (e.g., Pham et al., 2011; Xu et al., 2005). In the latter case one have to make sure that the integrity of the database is maintained. In simulations dealing with mineral reaction rates, the equilibrium constants for minerals, and the consistency of these, provide the direction of reaction and influence the rate which is a function of degree of under- or oversaturation (e.g., Lasaga, 1981; Aagaard and Helgeson, 1982). For minerals that are far-from-equilibrium undersaturated with respect to an aqueous solution, i.e., the aqueous activity product is less than the equilibrium constant, Lasaga (1981) and Aagaard and Helgeson (1982) suggested that dissolution rates become independent of the distance from equilibrium, whereas rates approach a linear dependence on the distance from equilibrium at close-to-equilibrium conditions (Fig. 1). The requirement of accurate thermodynamic data are therefore much higher for those minerals that are close to equilibrium than those that always stay far-from-equilibrium undersaturated. Examples of the latter are various clay minerals such as smectites and chlorites reacted at elevated CO_2 pressures (Pham et al., 2011), or forsterite (Mg_2SiO_4) that are known to always stay far-from-equilibrium undersaturated during surface weathering.

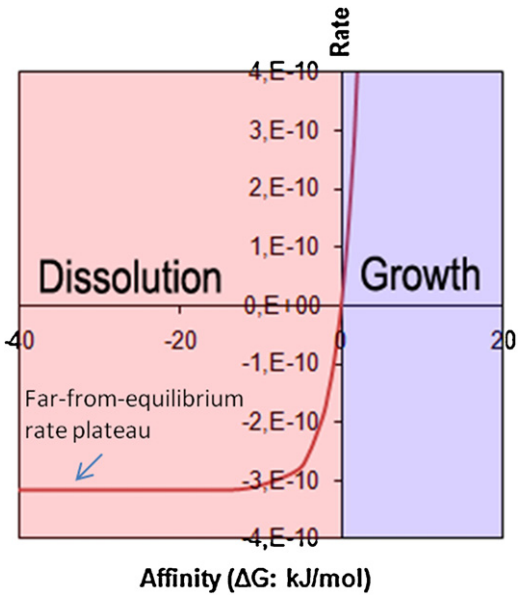

Fig. 1. Mineral reaction rates as a function of Gibbs free energy estimated by Eq. (1), at constant pH and assuming that rates are independent of solute activities. At far-from-equilibrium undersaturation, a plateau value is reached were rates are independent of the thermodynamic driving force.

As for thermodynamic data, dissolution rate data are available in various compilations. The most complete today is the one prepared by Palandri and Kharaka (2004) that consist of rate data for more that 70 minerals, including silicates, carbonates, oxides, etc. Data on mineral growth and nucleation rates are fewer, but data do exist for some silicates and hydroxides, and for carbonates such as calcite (Teng et al., 2000), magnesite (Saldi et al., 2009)

and dolomite (Arvidson and Mackenzie, 1999). The data available are mostly obtained from single-mineral far-from-equilibrium dissolution rate experiments done at various pH and with various concentrations of inhibiting or catalyzing solutes. These experiments are fairly simple and easier to do than for example growth rate experiments. As there has been a wide acceptance that theories such as TST are capable of predicting close-to-equilibrium dissolution and growth rates from the far-from-equilibrium dissolution rate data, less effort has been focused on mineral growth. Recently, comparisons of laboratory growth rates with rates predicted from dissolution rate data using the TST, suggest that other theories can better explain growth, and that more work is needed on mineral nucleation and growth to better predict the long-term potential for carbonate formation during CO_2 storage (Gaus et al., 2008; Hellevang and Aagaard, 2010).

3. What mineral reactions are important to consider?

When modelling CO_2–water–mineral interactions, the choice of primary and secondary minerals included in the simulations is a balance between the requirement of a complete representation of primary and possible secondary mineral phases, and the need to reduce the complexity to allow the numerical simulations to succeed. For closed-system zero-dimensional batch simulations of small-scale laboratory systems or reservoir volumes, a complete set of primary and secondary minerals with reaction rate equations for dissolution and growth can normally be solved with codes such as PHREEQC, even though the system defines highly stiff sets of ODE's. At the other end of the scale are 3D reactive-flow basin- or reservoir scale simulations, with little room for solving the kinetic equations. A number of problems end up between the two. In addition to the constraints imposed by spatial complexity, the choice of mineral reactions also depends on the temporal scale of interest. For long time scales, fast reacting minerals such as calcite ($CaCO_3$) can be regarded as reacting instantaneous and be regarded as equilibrium phases, whereas slow reacting phases such as quartz and some silicates can be neglected for short simulations. A guide to identify what geochemical reactions may be considered for various spatial scales and complexities, for various temporal scales, and for low and high temperatures, are summarized in Table 1. Note that for any reactive transport simulation, the aim should always be to provide a sufficient description of the CO_2–mineral–solution interactions to provide scientific sound results. At low degree of spatial complexity (e.g., 0D Batch to 2D radial), it is possible to solve computational costly stiff ODE systems together with the aqueous equilibrium speciation solved by Newton–Raphson (NR) iterations. At short time spans (e.g., <20 years) and low temperatures (<60–80 °C), it is however not necessary to consider slow reactions for most systems, and it is sufficient to take account for the calcium carbonate system, possible NaCl scaling, and if possible the dissolution of minerals such as glauconite, smectite and chlorite that may contribute significantly to carbonate storage (e.g., Pham et al., 2011). At longer time-scales, the number of minerals that may affect the reservoir properties and CO_2 storage increases. Climbing up one step in complexity (e.g., 2D simulations with complex geometry), results in less computer power available for solving the geochemical reactions. We therefore suggest the use of a semi-kinetic approach in this case. The semi-kinetic approach corresponds to a local equilibrium assumption (Helgeson, 1968), i.e., a few rate-controlling dissolving phases are solved according to reaction rate equations, whereas secondary phases are allowed to grow at equilibrium and hence be solved by NR iterations. The few rate equations solved in this case give an easy to solve non-stiff system of ODE's. Finally, for 3D reservoir or basin scale simulations with complex geometries, further simplifications may be required, and the aim should be to identify the major reactions and, if possible, simplify the rate formulations into analytical expression.

4. On solving mineral reaction rates

The most common way of modelling mineral dissolution and precipitation rates is using rate equations derived from transition state theory (TST) (Aagaard and Helgeson, 1982):

$$r_{+,-} = k_+ S \prod_i a_i^{\nu_+} \left(1 - \exp\left(\frac{\Delta G_R}{\sigma RT}\right)\right), \quad (1)$$

where, r is reaction rate (mol/s), k_+ is the forward (dissolution) reaction rate coefficient (mol/m^2 s), S is the reactive surface area (m^2), a is the activity of aqueous solute species i affecting the rates, ν is the reaction order, ΔG_R is the Gibbs free energy of the reaction, R is the gas constant, T is the absolute temperature, and σ is the Temkin's coefficient denoting the rate of the destruction of the activated complex compared to the overall reaction rate (values typically 1, 2, or 3; Schott et al., 2009). The k_+ most commonly used are those derived from laboratory experiments done at far-from-equilibrium undersaturated conditions and compiled in (Palandri and Kharaka, 2004). As sketched in Fig. 1, rates calculated with Eq. (1) approach a plateau value as exp ($\Delta G_R/RT$)

Table 1
Choice of minerals to include and solution methods (NR, Newton–Raphson algorithm used for equilibrium calculations; ODE, ordinary differential equations used to define mineral reaction rates; analytical, first-order decay equation used for dissolving phases at far-from-equilibrium undersaturation) based on the time of interest, temperature, system size, and geometrical complexity.

Spatial scale	Temporal scale	Temperature	Chemistry	Solution method
3D Reservoir/Basin (complex geometry)	Short (<20 years)	Low (<60–80 °C)	Calcite dissolution, pH changes, NaCl scale	NR + analytical
		High (>60–80 °C)		
	Long (100s years)	Low (<60–80 °C)		
		High (>60–80 °C)		
2D (Complex geometry)	Short (<20 years)	Low (<60–80 °C)	Calcite dissolution, pH changes, NaCl scale	NR + analytical
		High (>60–80 °C)	Few minerals + all aq. species	NR + semi-kinetic
	Long (100s years)	Low (<60–80 °C)	All minerals (– dolomite, magnesite, quartz) All aq. species	NR + semi-kinetic
		High (>60–80 °C)	All minerals + all aq. species	
0D Batch 2D radial	Short (<20 years)	Low (<60–80 °C)	Calcite dissolution, pH changes, NaCl scale	NR + analytical
		High (>60–80 °C)	All minerals + all aq. species	NR + ODE solver (stiff) (fully kinetic approach)
	Long (100s years)	Low (<60–80 °C)	All minerals (– dolomite, magnesite, quartz) All aq. species	NR + ODE solver (stiff) (fully kinetic approach)
		High (>60–80 °C)	All minerals + all aq. species	

approaches zero. For growth, Eq. (1) calculates rapid rates down to low supersaturation (Fig. 1). The activity product term of has commonly been used to define the pH ($-\log(a_{H^+})$) dependence of dissolution rates, and the rate data compilation (Palandri and Kharaka, 2004) therefore provides the pH dependencies for a large number of minerals. The activity term can also be used to incorporating inhibiting or catalytic effects of other aqueous solutes, and this has been used to explain effect of ions such as magnesium (Saldi et al., 2007) and aluminium (Lowson et al., 2005; Oelkers and Gislason, 2001; Oelkers et al., 1994) on dissolution rates. Although the use of Eq. (1) to predict rates as a function of distance from equilibrium is supported by a range of dissolution rate studies (e.g., Gautier et al., 1994; Pokrovsky and Schott, 2004; Saldi et al., 2010), there are some major challenges in using equations such as Eq. (1).

First, as rate coefficients are normalized to experimental surface areas, proper reactive surfaces have to be defined for the modelled natural reactions. For dissolution, the common choice is to use surface areas measured by the Brunauer–Emmet–Teller (BET) (Brunauer et al., 1938) method (e.g., Pham et al., 2011), or to use geometric models with surface areas adjusted to include factors such as surface roughness, mineral shape, or secondary mineral coatings (e.g., Gaus et al., 2005a; Knauss et al., 2005; Xu et al., 2005). This is a common challenge when solving any macroscopic rate equation describing mineral dissolution, and there is no single general solution. Some of the factors that are believed to influence the reactivity of mineral surfaces are surface ageing and reaction history (Arvidson and Luttge, 2010; Lüttge, 2006), and the formation of secondary coatings (e.g., Béarat et al., 2006). These factors, together with variations in grain size distributions, make predictions very challenging. For the formation of secondary phases, here defined as minerals with zero initial mass, estimates of reactive surface areas are even more challenging. The common approach is to use a reactive surface area for growth that is a fraction of the total sediment surface area (e.g., Gaus et al., 2005a). This is highly unphysical as growth of a mineral phase is only related to the reactive surface of the phase itself, and not dependent on the substrate. The role of the substrate is to provide surface for heterogeneous nucleation of the secondary minerals. As mineral nucleation cannot be modelled with Eq. (1), the solution is to add a proper nucleation rate term (Steefel and Van Cappellen, 1990).

A second challenge is found in the activity term of Eq. (1). As mineral dissolution commonly is seen mechanistically as exchange reaction between aqueous protons and surface metal cations (Gautier et al., 1994; Oelkers and Gislason, 2001; Oelkers et al., 1994), the ion activities occur as ratios of the proton activity over the cation M^{N+}:

$$r_{+/-} = k' \left(\frac{a_{H^+}^N}{a_{M^{N+}}} \right)^n, \quad (2)$$

where k' is a rate constant (mol/s) and n is an empirical derived parameter. It is clear that great care has to be taken in using rate equations of this form. For example will a simulation of a rock initially interacting with freshwater or where the cation M^{N+} has been defined to have zero initial concentration, cause infinite dissolution rates at the initial time step.

A third challenge comes from the assumption that one single mechanism is responsible for the rates at any distance from equilibrium, and that far-from-equilibrium dissolution rate mechanisms therefore may be used to predict growth rates. This prediction is counterintuitive, and recent advances in the understanding of mineral reaction rates and comparisons of growth rates with rates predicted from dissolution rate data using the TST, suggest that other theories can better explain dissolution and growth (Arvidson and Luttge, 2010; Dove et al., 2005; Luttge, 2005; Teng et al., 2000). We illustrate the discrepancy between TST-predicted and measured growth rates by using magnesite and dolomite rates as examples (Fig. 2). Data for magnesite growth at 100 °C as a function of oversaturation is reported from hydrothermal atomic force microscopy (HAFM) studies and mixed-flow laboratory experiments in (Saldi et al., 2009) (Fig. 2a). These data suggest that the growth of magnesite is controlled by spiral growth and that the growth can be approximated by a function that is second-order with respect to affinity and with a growth rate coefficient of 6.5×10^{-12} mol/m^2 s (Fig. 2a). Magnesite dissolution rate data at 100 °C is reported in (Pokrovsky et al., 2009) and suggests a far-from-equilibrium dissolution rate coefficient of 3.16×10^{-8} mol/m^2 s. Using the TST equation with constant solute activities to extrapolate this to growth rates, leads to orders of magnitude faster rates than given by the growth rate experiments (Fig. 2a). A similar result is obtained for dolomite

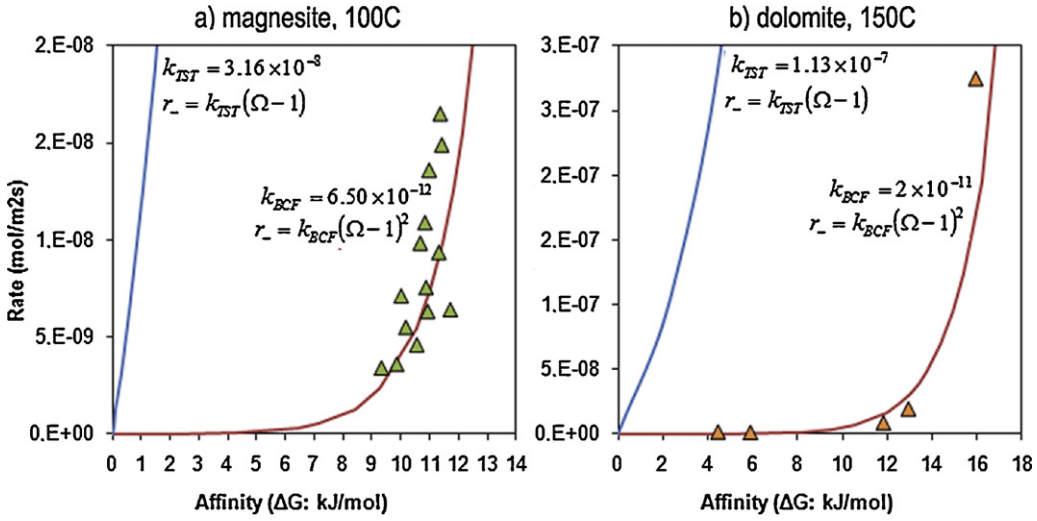

Fig. 2. Comparisons of actual growth rate data with extrapolations using Eq. (1) for (a) magnesite; and (b) dolomite. Dissolution rate data used for the extrapolation are from Pokrovsky et al. (2009), whereas growth rate data for magnesite and dolomite are from Saldi et al. (2009) and Arvidson and Mackenzie (1999) respectively. The comparisons suggest that the transition-state-theory extrapolations overestimate the growth rates at low supersaturations by ~4 orders of magnitude.

with rate coefficients for dissolution and growth that diverge by approximately four orders of magnitude at 150 °C (Fig. 2b). Moreover, as the activation energies reported for magnesite and dolomite growth (Arvidson and Mackenzie, 1999; Saldi et al., 2009) are significantly higher than those reported for dissolution (Pokrovsky et al., 2009), the difference between growth data and TST predictions diverge further at lower temperatures. Generally, laboratory methods such as AFM, that can directly monitor dissolving and growing surfaces, suggest that the mechanisms responsible for dissolution and growth are different, and that growth rates should therefore be modelled by non-linear growth models, such as given by Burton–Cabrera–Frank (BCF) (Burton et al., 1951), rather than the by the linear TST that may work well for dissolution.

Limitations of Eq. (1), such as overpredictions of growth rates by orders of magnitude, and the lack of proper reactive surface areas of secondary phases initially with zero mass, may have resulted in poor estimates of the nature and magnitude of mineral reactions following CO_2 storage (Hellevang and Aagaard, 2010; Pham et al., 2011). To overcome some of the limitations of Eq. (1), we suggest to define separate equations for dissolution and growth rates, and to include a nucleation rate term to generate mass and surfaces for mineral growth. The equations should be as simple and general as possible to allow them to be included in numerical tools, but the equations should still provide reliable data. Steefel and Van Cappellen (1990) suggested a model consisting of a second-order growth model coupled with a nucleation rate term. In their model, the reactive surface areas of growth were properly estimated by taking account of the particle size distributions. This model is general and overcomes most of the limitations of Eq. (1), but is too complex with too many parameters to easily fit into numerical tools such as TOUGHREACT (Xu et al., 2011). A simplified model was therefore suggested by Hellevang and Aagaard (2010) and later used to model the long-term potential for carbon storage in the Sleipner CO_2 injection (Pham et al., 2011). For dissolution rates, Eq. (1) is used, whereas growth is modeled by a second-order term and nucleation rates are estimated according to a term simplified from classical nucleation rate theory:

$$-\frac{dn}{dt} = k_{-}S\{\Omega - 1\}^2 + k_N \exp\left\{-\Gamma_{ij}\left(\frac{1}{(T)^{3/2}\ln\Omega}\right)^2\right\}, \quad (3)$$

where k_{-} is the growth rate coefficient (mol/m^2 s), S is the reactive surface area, $\Omega = \exp(\Delta G_R/RT)$ is the saturation state, k_N is the nucleation rate coefficient (mol/s), and Γ_{ij} is a constant where nucleation rate parameter such as surface tension, molar volume, and the geometric surface shape factor have been lumped together (Pham et al., 2011). By running a sensitivity test on the nucleation rate parameters, Pham et al. (2011) showed that the model was highly sensitive to changes in Γ, with reasonable values for carbonates such as magnesite, dolomite and siderite in the range 10^{10} to 5×10^{10} (using $k_N = 1$ mol/s). The subscript ij used for Γ denotes pair coefficients between nucleating phases and substrate, and illustrates the dependence of nucleation rates on interfacial tensions. These values are uncertain, and we recommend running sensitivity tests on Γ. The reactive surface area for dissolution and growth per volume aqueous solution is a function of the particle size distribution and the fraction of the total surface area that is reactive. If a particle size distribution is not available, the reactive surface area can be approximated by:

$$S = \lambda n M \beta, \quad (4)$$

where n is mole, M is the molar weight, β is the specific surface area, and λ is the reactive fraction of the total surface area of the mineral. Commonly, λ is assumed to be one, and the specific surface area is approximated by a BET value, or a geometric value (e.g., assuming perfectly spherical particles, cubes, plates, etc.) multiplied with a surface roughness factor.

5. Examples of geochemical modelling of CO_2–water–rock interactions

To illustrate how information on geochemical reactions can be obtained for various temporal and spatial scales and complexities, we performed equilibrium calculations, semi-kinetic and fully kinetic numerical simulations using the PHREEQC v2 (Parkhurst and Appelo, 1999) numerical code. The simulations are closed-system batch simulations and cannot be used to explore reaction–diffusion–flow relations, but are instead used to estimate CPU times for each type of simulation, and to propose a guide of simulation strategy for the more complex systems.

For the thermodynamic calculations, the standard state adopted in this study was that of unit activity for pure minerals and H_2O at any temperature and pressure. For aqueous species other than H_2O, the standard state was unit activity of the species in a hypothetical 1 molal solution referenced to infinite dilution at any temperature and pressure. For gases, the standard state was for unit fugacity of a hypothetical ideal gas at 1 bar of pressure. The thermodynamic and kinetic calculations were performed using the geochemical code PHREEQC-2 (Parkhurst and Appelo, 1999) with the llnl.dat database based on the thermo.com.V8.R6.230 dataset prepared at the Lawrence Livermore National Laboratory. Because glauconite ($Ca_{0.02}K_{0.85}Fe_{1.03}Mg_{1.01}Fe_{0.05}Al_{0.32}Si_{3.735}O_{10}(OH)_2$) and ankerite ($CaFe_{0.6}Mg_{0.4}(CO_3)_2$) is not included in the llnl.dat database, we estimated the equilibrium constants for these two phases as described in Pham et al. (2011). As the ideal gas law is used in PHREEQC-2, input partial pressures were corrected for by a fugacity coefficient and a poynting correction term to make CO_2 solubility calculations accurate. The fugacity coefficient of CO_2 was calculated by the Soave–Redlich–Kwong (SRK) equation of state (Soave, 1972).

We used the temperature (37 °C), pressure (100 bar), initial formation water chemistry and mineralogy reported for the Utsira Reservoir at the Sleipner injection site (see Pham et al., 2011) for the simulations. This reservoir provides a good example of a low-temperature system, where the significance of slow growth reactions such as magnesite and dolomite can be identified in the fully kinetic approach and from this be considered for the semi-kinetic simulations. The system also illustrates well the challenges of modelling low-temperature growth of silica polymorphs, where the less crystalline low-stability phases are known to form rather than quartz. The initial mineralogy and secondary phases with kinetic parameters used for Eqs. (1) and (3) are summarized in Table 2, whereas Table 3 gives the mineral chemistry and amount of divalent metal cations provided per mole mineral reacted. The system was simulated for 10,000 years of CO_2–water–mineral interactions.

5.1. Fully kinetic approach

In this section we divided the simulations into two different runs to illustrate the sensitivity of quartz growth rates on secondary carbonate formation, and one series of batch simulations with different CO_2 pressures to see the effect on mineral saturation states and reaction rates. The PHREEQC input for the 100 bar CO_2 no-quartz-growth case is provided as an electronic Supplementary data file.

The thermodynamic stability of dissolving primary source minerals such as feldspars and clay depend strongly on the silica activity. For example, dissolution of albite ($NaAlSi_3O_8$) releases

Table 2
Kinetic parameters for Eqs. (1) and (3).

Mineral	k_+ (mol/m^2 s)[a]	$E_{a,+}$ (kJ/mol)	k_- (mol/m^2 s)[a]	$E_{a,-}$ (kJ/mol)	Γ (Pham et al.)	S (m^2/g)
Quartz (Rimstidt and Barnes, 1980)	4.5×10^{-14}	72.0	1.4×10^{-13}	49.8	4×10^{10}	0.02
Chalcedony (Rimstidt and Barnes, 1980)	5.2×10^{-14}	62.9	1.4×10^{-13}	49.8	2×10^{10}	0.02
Albite (Brantley, 2008)	1.1×10^{-12}	65.0	–	–	2×10^{10}	0.1
K-feldspar	2.3×10^{-13} (Brantley, 2008)	51.7 (Palandri and Kharaka, 2004)	–[c]	–	2×10^{10}	0.11 (Gautier et al., 1994)
Glauconite	1.3×10^{-10} (Aagaard et al., 2004)	85.0 (Palandri and Kharaka, 2004)	–	–	2×10^{10}	0.018 (Tardy and Duplay, 1994)
Clinochlore-14A	7.1×10^{-13} (Brandt et al., 2003)	88.0 (Nagy, 1995)	–	–	2×10^{10}	1.6 (Brandt et al., 2003)
Smectite-high-Fe-Mg	1.8×10^{-14} (Golubev et al., 2006)	71.1 (Amram and Ganor, 2005)	–	–	2×10^{10}	48 (Golubev et al., 2006)
Kaolinite (Yang and Steefel, 2008)	1.2×10^{-13}	29.3	5.8×10^{-15}	–	2×10^{10}	
Muscovite (Oelkers et al., 2008)	3.1×10^{-14}	58.2	–	–	2×10^{10}	0.68
Magnetite (White et al., 1994)	1.0×10^{-10}	18.6	–	–	2×10^{10}	0.10
Pyrite (Palandri and Kharaka, 2004)	9.6×10^{-11}	56.9	–	–	2×10^{10}	0.051
Calcite	Equilibrium	–	Equilibrium	–	–	–
Ankerite[b]	–	–	–	–	3×10^{10}	–
Siderite (Golubev et al., 2009)	1.3×10^{-7}	48.0	–[c]	–	2×10^{10}	0.18
Magnesite	2.5×10^{-9} (Pokrovsky et al., 2009)	34.0	1.6×10^{-17} (Saldi et al., 2009)	159.0 (Saldi et al., 2009)	4×10^{10}	0.13 (Pokrovsky et al., 2009)
Disordered dolomite	9.4×10^{-8} (Pokrovsky et al., 2009)	21.0	4.5×10^{-25} (Arvidson and Mackenzie, 1996)	133.5 (Arvidson and Mackenzie, 1999)	4×10^{10}	0.016 (Pokrovsky et al., 2005)
Dawsonite (Hellevang et al., 2010)	1.8×10^{-9}	63.8	–[c]	–	2×10^{10}	9.8

[a] k_+ and k_- are reaction rate coefficients at 25 °C at pH 5.
[b] No data available and rate therefore assumed intermediate between siderite and dolomite.
[c] No data available and growth rate coefficient therefore assumed equal to the TST dissolution rate coefficient.

Table 3
Mineral names, chemical formulas and number of moles metal cations released for each mole of mineral dissolved.

Mineral name	Chemical formula	Sum divalent metal cations/mole mineral
Quartz	SiO_2	0
Chalcedony	SiO_2	0
Albite[a]	$NaAlSi_3O_8$	0
K-feldspar	$KAlSi_3O_8$	0
Glauconite	$Ca_{0.02}K_{0.85}Fe_{1.03}Mg_{1.01}Fe_{0.05}Al_{0.32}Si_{3.735}O_{10}(OH)_2$	2.11[b]
Clinochlore-14A	$Mg_5Al_2Si_3O_{10}(OH)_8$	5
Smectite-high-Fe-Mg	$Ca_{0.025}Na_{0.1}K_{0.2}Fe_{0.5}Fe_{0.2}Mg_{1.15}Al_{1.25}Si_{3.5}H_2O_{12}$	1.875[b]
Kaolinite	$Al_2Si_2O_5(OH)_4$	0
Muscovite	$KAl_3Si_3O_{10}(OH)_2$	0
Magnetite	Fe_3O_4	3[b]
Pyrite	FeS_2	1
Calcite	$CaCO_3$	1
Ankerite	$CaFe_{0.6}Mg_{0.4}(CO_3)_2$	2
Siderite	$FeCO_3$	1
Magnesite	$MgCO_3$	1
Disordered dolomite	$MgCa(CO_3)_2$	2
Dawsonite	$NaAl(OH)_2CO_3$	

[a] Albite supply Na and Al for potential dawsonite growth.
[b] Assuming all released iron is reduced to Fe^{2+}.

3 mol of silica per mole mineral and the activity product is given by:

$$q_{alb} = a^3_{SiO_{2,aq}} \frac{a_{Na^+} a_{Al^{3+}}}{a^4_{H^+}}, \quad (5)$$

and the Gibbs free energy for the reaction is:

$$\Delta G_r = \Delta G^0_r + RTln\, q_{alb}, \quad (6)$$

where superscript 0 denotes standard-state. It is generally accepted that quartz rates at low temperatures (<60 °C) are very slow, and it is common to find systems reaching high silica super saturation at low-temperatures (Bjorlykke and Egeberg, 1993). It is therefore common to model silica growth in reservoirs such as Utsira Sand by assuming a zero growth rate for quartz and allow chalcedony or amorphous silica to grow instead (e.g., Pham et al., 2011). This assumption is however not supported experimentally (see quartz growth rates by Rimstidt and Barnes (1980) and challenging if extrapolated to very long time scales (e.g., Steefel and Van Cappellen, 1990). Hellevang et al. (2011) showed that at high aqueous silica activities, supersaturated with respect to quartz, albite was stabilized and dawsonite ($NaAl(OH)_2CO_3$) was prevented to form. Therefore, at slow quartz growth rates, the potential for carbonate formation in divalent metal-cation poor reservoirs like Utsira was strongly reduced. Here, to illustrate the sensitivity of the reactions on quartz growth rates we divided the simulations into one where no quartz were allowed to form, and one with a quartz growth rate based on the Rimstidt and Barnes model (Rimstidt and Barnes, 1980).

The temporal evolution of selected minerals and the corresponding saturation states for the no-quartz run are shown in Fig. 3. The simulation shows that minerals like smectite ($Ca_{0.025}Na_{0.1}K_{0.2}Fe(II)_{0.5}Fe(III)_{0.2}Mg_{1.15}Al_{1.25}Si_{3.5}H_2O_{12}$), chlorite ($Mg_5Al_2Si_3O_{10}(OH)_8$), and glauconite dissolves completely within approximately 100 years (Fig. 3a), releasing Mg, Fe, and Ca that stabilize carbonates such as ankerite, siderite ($FeCO_3$), magnesite ($MgCO_3$) and dolomite ($MgCa(CO_3)_2$) (Fig. 3d). All other silica reactions are slow and are not shown here. For a full review of these reactions we refer to Pham et al. (2011). As nucleation is required before the secondary phases grow (Eq. (3)), there is a lag period of approximately 5 years before ankerite starts growing (Fig. 3c). At this point the saturation states of secondary carbonates drops and only ankerite grows at any significant amount. It is interesting to note that most of the Ca^{2+} supplied for ankerite growth was supplied from dissolving calcite ($CaCO_3$). From Fig. 3b it is clear that the saturation states of smectite, chlorite, and glauconite are far from equilibrium undersaturated during the whole period. Therefore, for these phases, Eq. (1) can be simplified to $r = k_+ S a^n_{H^+}$, and further simplified to $r = k'_+ S$, where k'_+ is the rate constant at the given pH, if the pH is nearly constant during the simulated time. The latter has a simple analytical solution given by a first order decay equation, and the moles of the minerals at the end of a time step can hence be calculated by:

$$n(t) = n_0 \exp(-M\beta k'_+ t), \quad (7)$$

where n_0 is the moles of the mineral at the start of the time step, M is molar mass of the mineral, β is the specific surface area, and t is size of the time step. The half-time (time required to dissolve half of the mass) of the mineral can now easily be calculated by a rearranging Eq. (7).

The same simulation as for the above was done using quartz growth rates extrapolated from Rimstidt and Barnes (1980). Because quartz required a long induction time before significant growth, there was no difference in the first 6000–7000 years. After this time however, quartz started growing and the activity of aqueous silica was reduced. As the silica activity dropped, albite ($NaAlSi_3O_8$) was destabilized and dissolved faster, and dawsonite started growing from the released Na and Al (Fig. 4). Fig. 4b shows how the dawsonite growth rate is coupled to the growth rate of quartz, even though they do not share any common elements. The lowering of silica activity and destabilization of albite led in this case to significant more dawsonite formed, and to a corresponding increase of the total amount of carbon stored as secondary carbonates (Fig. 5).

We showed that for primary phases such as smectite, chlorite, and glauconite that are always far-from-equilibrium, we can replace the ODE's by simple first-order decay equations such as Eq. (7). As the saturation states are dependent on the CO_2 pressure, we performed a series of batch simulations with varying CO_2 pressures. We used the same system as simulated above with no quartz growth. Fig. 6 shows the saturation states for glauconite, smectite, and chlorite over 10,000 years for CO_2 pressures from 1 to 100 bar. For the three minerals we see that the maximum saturation is given for at 1 bar CO_2 pressure, with glauconite and smectite reaching SI ($\Omega = 10^{SI}$) values between 0 and −1. This is however over a very short time, and the saturation states stay <−1 for the remaining of the simulations. As a value of SI = −1 gives 90% of the full far-from-equilibrium dissolution rate, we conclude that the dissolution rates for these three phases can be simplified to a first-order decay even down to low CO_2 pressures.

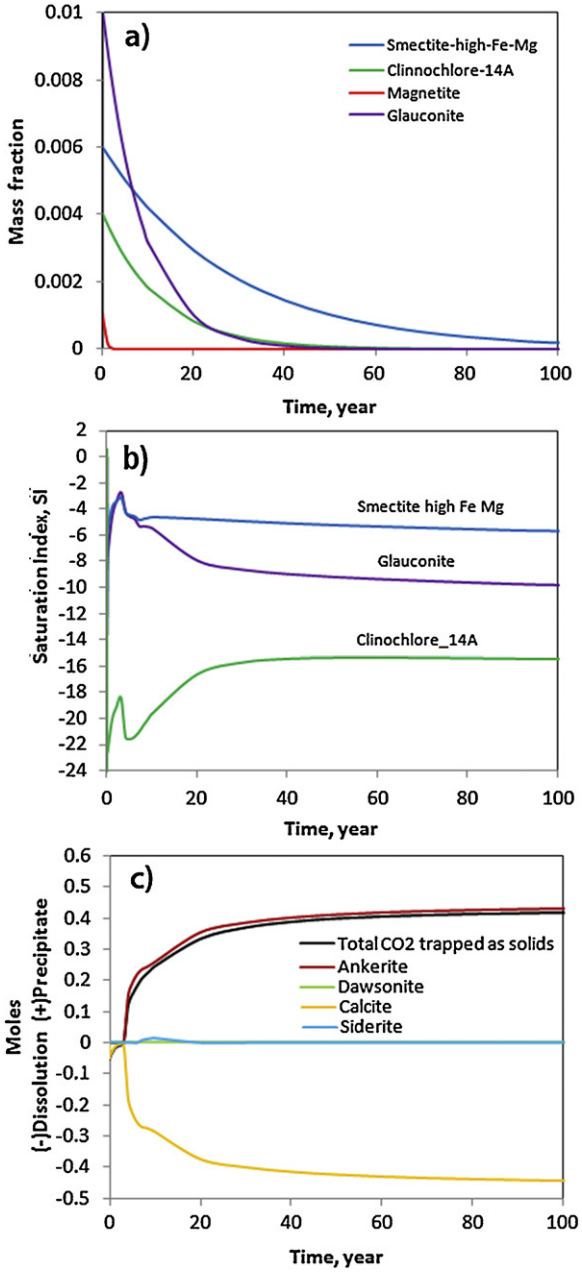

Fig. 3. Simulation where all mineral reactions were solved according to rate Eq. (1), except for calcite which was assumed to be at local equilibrium. The PHREEQC data corresponds to those used in Pham et al. (2011). The results of this fully kinetic simulation were used as benchmark values to compare subsequent simulations with various degrees of simplifications. (a) smectite, clinochlore, magnetite, and glauconite dissolved to completion within ~100 years providing divalent cations for secondary carbonate growth; (b) the saturation state of the minerals never reached values higher than ~−2 and were therefore independent of the thermodynamic driving force ($1 - \exp(\Delta G_R/RT) = 1$); and (c) ankerite formed from the release of divalent cation, aluminium and sodium. Calcite dissolved and released Ca^{2+} for ankerite.

For this system (low temperature), the fully kinetic simulations support that phases such as magnesite and dolomite can be neglected as possible secondary phases as proposed in Table 1 (see also discussions in Pham et al., 2011). We also advice that dawsonite is not included for short-term simulations as this phase has not yet been shown to form experimentally at low temperatures in acidic solutions (see Hellevang et al., 2011 and Kaszuba et al., 2011 for a discussion on the stability of dawsonite). Moreover, although growth rate data provided by Rimstidt and Barnes (1980) support quartz growth down to low temperatures, the evidence for

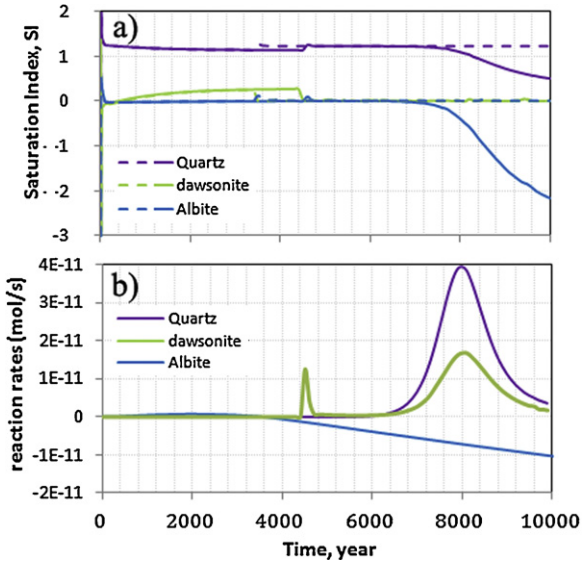

Fig. 4. The effect of quartz growth rates on the formation of dawsonite. (a) For the base-case (dashed curves) quartz were not allowed to form, and albite stayed stable close-to-saturation. With quartz allowed to form according to rates estimated from Rimstidt and Barnes (1980), silica and albite activities dropped; (b) as quartz started to form, albite got unstable and dissolved. With the increased rate of aluminium addition to the solution, dawsonite growth accelerated proportionally to the quartz growth rates, before the system relaxed and rates slowed down close to equilibrium.

quartz-supersaturated solutions at low temperatures are compelling, and we therefore advice to use chalcedony or amorphous silica as secondary silica species and reduce quartz growth rates by orders of magnitude to allow quartz supersaturated solutions. The runtime for one fully kinetic batch simulation on a single Intel© Xeon© 2.66 GHz CPU was typical 2–4 h.

5.2. Semi-kinetic approach

To compare how well the semi-kinetic approach compares to the fully kinetic simulations, we used the same system as for the previous section, but with only chlorite, smectite, glauconite, albite and magnetite as kinetic phases and the remaining minerals allowed to dissolve and form at equilibrium (i.e., a local equilibrium assumption). The kinetic phases were selected as those phases that were undersaturated for the entire fully kinetic simulations, and that contributed to the bulk of secondary carbonate formation. Because dawsonite was suggested to form at the later stage of the

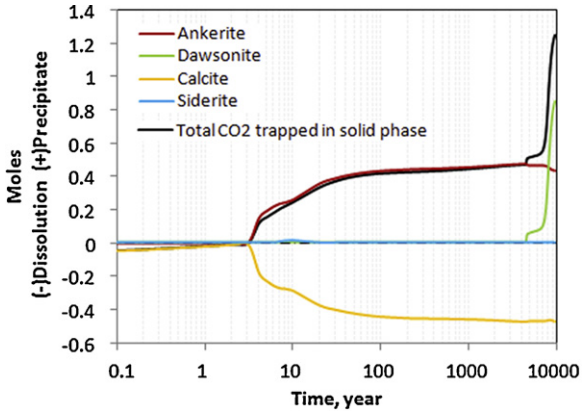

Fig. 5. The potential for secondary carbonate formation for a low-temperature system allowing quartz growth according to Rimstidt and Barnes (1980). We see that the quartz growth allows a significant amount of dawsonite to form at the late stage of the simulated time.

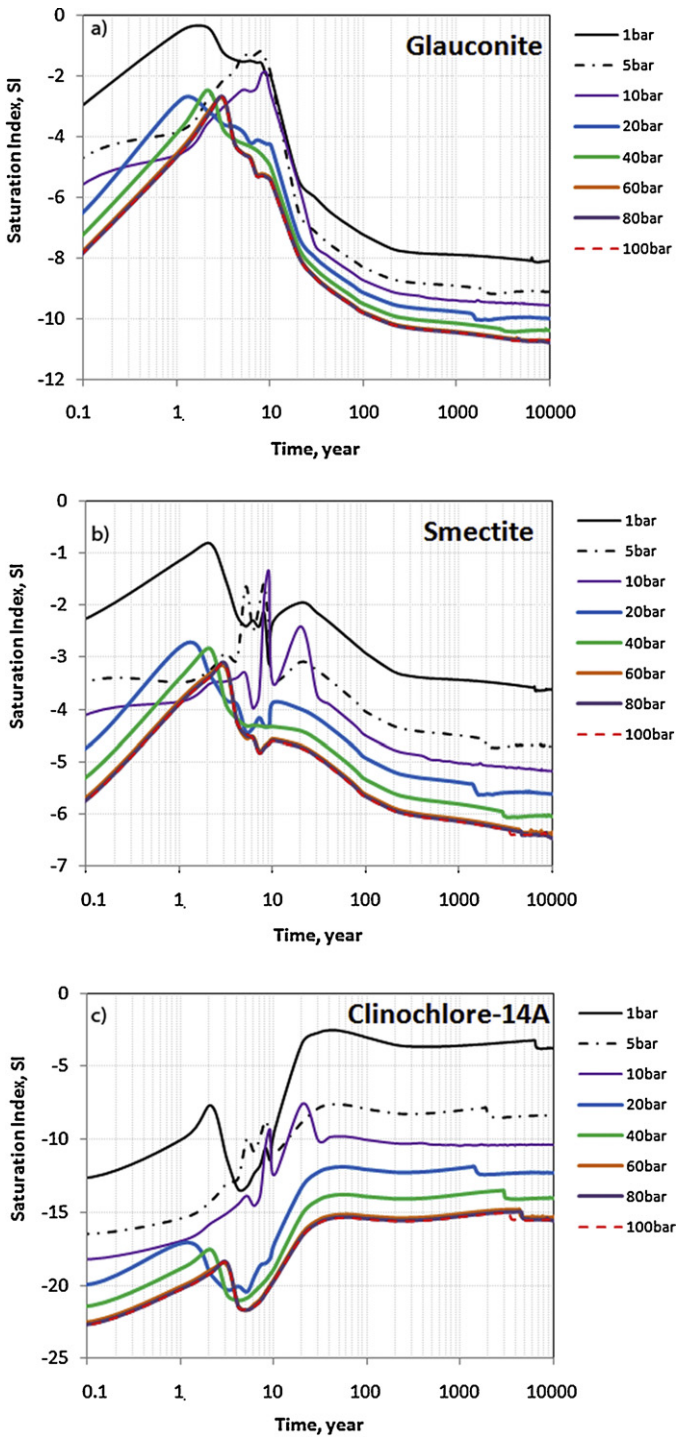

Fig. 6. The effect of CO_2 pressure on the saturation states of (a) glauconite; (b) smectite; and (c) chlorite. For the lowest CO_2 pressures, glauconite and smectite approach equilibrium for a brief time before the saturation states drops to far-from-equilibrium conditions for the remaining simulated times. The simulations suggest that these three minerals can be treated as far-from-equilibrium phases down to low CO_2 pressures, which allows for further simplifications such as into first-order decay equations for large-scale simulations.

10,000 years simulations (Figs. 3–5) we attempted to include dawsonite in the equilibrium assemblage. This forced the solution to be in equilibrium with the primary minerals K-feldspar and kaolinite together with dawsonite, and resulted in instantaneous growth and a large amount of dawsonite formation compared to the fully kinetic approach. Because no growth or nucleation rate data are known for dawsonite, the potential for dawsonite to store CO_2 is not known. The fact that dawsonite is thermodynamically stable suggests however that it should be considered as a potential secondary phase.

To illustrate how well the two approaches compare, we show the predicted amount of ankerite that forms and the pH evolution at 100 and 5 bar (Fig. 7a and b). At 100 bar, after a few years, the two approaches compare very well for both pH and amount of ankerite formed (Fig. 7a and c). The deviation is larger for 5 bar, especially for the predicted amount of ankerite formed (Fig. 7b and d). At low CO_2 pressures, the pH is higher and a larger amount of ankerite form because pyrite is less stable and more iron is released and made available. The largest difference between the semi- and fully kinetic approaches is seen for the first few years. Whereas the fully kinetic approach does not predict any significant carbonate growth as the secondary phases require nucleation before growth, the local equilibrium assumption predicts instantaneous rapid growth (Fig. 7a and b). The deviation between the two methods are therefore large, and the use of the local equilibrium assumption to predict secondary carbonate formation for short time spans should be done with great care (see also Gaus et al., 2005a). For the long-term predictions (>10 years), although with some difference especially at low CO_2 pressures, the semi kinetic approach is still suggested to provide a good approximation if the fully kinetic simulation can not be used. The most important reason for using the simpler semi kinetic approach is to reduce the run time. For the present simulations, the semi kinetic approach, using a single Intel© Xeon© 2.66 GHz CPU, used 1–4 seconds for the full 10,000 years simulations. This is impressive 1800–14,400 times faster than the full kinetic simulations presented in the previous section.

5.3. Other approximations

If a ODE solver is not available, or if the system is too complex to include ODE's for the mineral reactions, or finally if the timing of carbonate formation is not important and only information on the total long-term potential (thousands of years) of mineral carbon storage is required, valuable information can be obtained by using simple hand calculations or simple equilibrium simulations. Table 4 shows such a simple calculation for ankerite that was shown in the previous section to be closely approximated by just taking into account the dissolution of glauconite, chlorite, magnetite, smectite, and pyrite. In the table the fraction x of the mineral dissolved is given, and we see that all minerals dissolve completely, except for pyrite which only dissolves 10% (Table 4). This value for maximum pyrite dissolution was provided from the fully kinetic simulations. If we use these values we achieve the same amount of ankerite formed as for the fully kinetic simulation, i.e., ~0.48 mol (Table 4). Calcium is assumed to be unlimited supplied and is hence not included in the calculations. If we do not have any information of the extent of pyrite dissolution and we hence assume 100% dissolution, the ankerite formation potential is instead limited by the supply of Mg, and we achieve ~0.94 mol of ankerite formed. If we also assume that all albite is converted into dawsonite, we obtain a maximum potential of 0.56 mol of dawsonite formed. Recalculated to total mass of CO_2 stored per sediment volume (35% porosity; 1 l aqueous solution; V_{sed} = 2.86 l), we obtain 82.7 g contribution from the ankerite and 24.7 g from dawsonite.

Another approximation is to use the semi-kinetic approach, but replace the ODE's with first-order decay equations. We saw that this is possible when the dissolving minerals are sufficient undersaturated and the rates become independent of the thermodynamic driving force and only dependent on the mass. We tested this approximation by doing a simple hand calculation where the dissolution of smectite, chlorite, glauconite, and magnetite

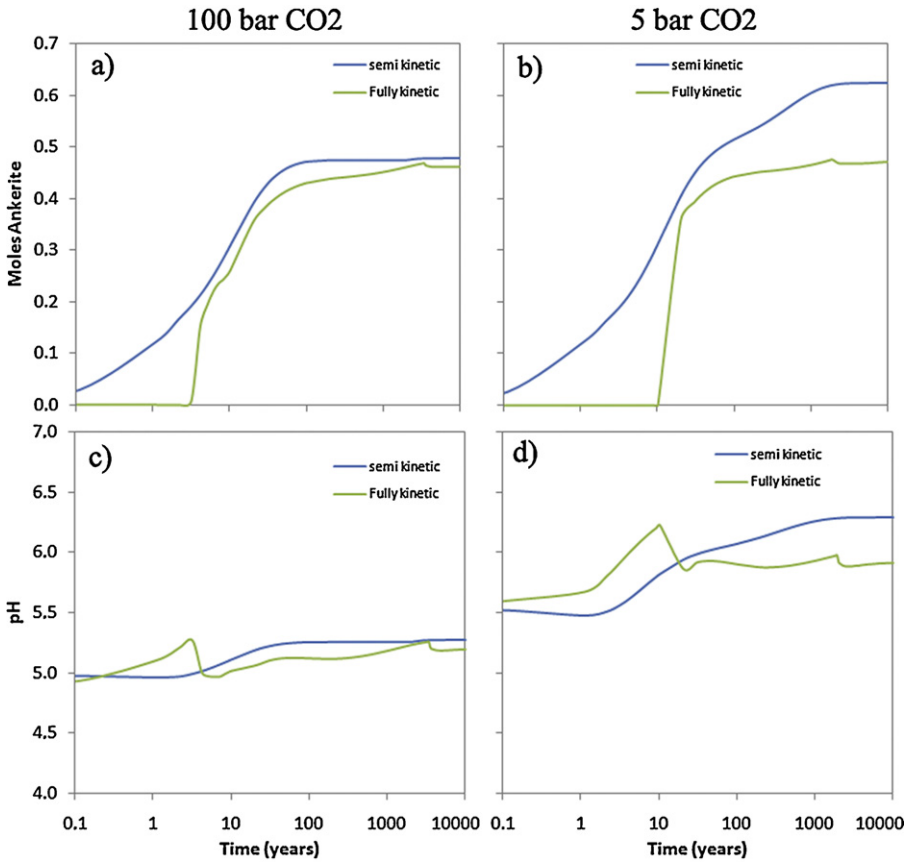

Fig. 7. Comparison between the semi-kinetic (local equilibrium assumption) and the fully kinetic simulations on the amount of ankerite formed and pH for CO_2 pressures of 100 and 5 bar: (a, c) at 100 bar, after ~5 years, both moles ankerite formed and pH compares well between the two models. Before this time, no ankerite formed in the fully kinetic simulation as this simulation mode required nucleation preceding the growth; (b, d) at 5 bar the difference between the two models are larger, mostly caused by a higher pH and a corresponding increase in the amount of pyrite dissolved at local equilibrium.

was defined as first-order decaying minerals using Eq. (5), and formation of ankerite was constrained by the amount of iron released. As mentioned in the previous paragraph, to estimate the amount of ankerite formed we do need to take into account pyrite dissolution. For these calculations we used a constant amount of iron released from pyrite that corresponded to the approximation done for the equilibrium calculations in the previous paragraph, i.e., 0.0491 mol. The mineral changes estimated by the semi kinetic approach and the hand calculations are shown in Fig. 8. The figure shows that the dissolution rates of smectite, chlorite, and glauconite solved by the ODE solver are nearly perfectly matched by the hand calculations assuming first-order decay (Fig. 8a). A comparison of the two models on the amount of ankerite formed again show a good match (Fig. 8b), but with some deviation which can be explained by a variable amount of pyrite dissolved in the semi-kinetic approach, whereas the hand calculations assumed a constant value. The close match between solving the ODE's defined by Eq. (1) and the first-order decay approximation shows that, as previously suggested, smectite, chlorite, magnetite, and glauconite are far enough undersaturated so that the rates are independent of the thermodynamic driving force. Note that caution has to be made for minerals like feldspars, as the mineral rates may show dependencies on solute activities at constant pH and saturation (e.g., Oelkers et al., 1994), and that the mechanisms of dissolution may vary as a function of saturation and hence give rate dependencies on the saturation state even at far-from-equilibrium undersaturation (e.g., Hellmann et al., 2010). However, for now we assume that the dissolution rates at constant pH for most minerals at far-from equilibrium undersaturation can be approximated by first-order decay equations.

Table 4
The long-term potential of carbonate formation as ankerite using equilibrium calculations and assuming a complete dissolution of the primary minerals, except pyrite that was dissolved 10% (according to the fully kinetic simulations). The amounts of ankerite formed assumed an ankerite of composition of $CaFe_{0.6}Mg_{0.4}(CO_3)_2$, and a potential value of 0.48 mol/kgw was estimated from the amount of Fe released (the limiting element in this case).

		Mol/kgw $t=0$	γ^a Fe	γ^a Mg	x Dissolved[b]	Mol Fe/kgw	Mol Mg/kgw
Glauconite	0.1152	1.08	1.01	1	0.124	0.116	
Smectite		0.0729	0.7	1.15	1	0.0510	0.0838
Chlorite		0.0354	0	5	1	0	0.177
Pyrite		0.1638	3	0	0.1	0.0491	0
Magnetite	0.0212	3	0	1	0.0636	0	
Sum						0.288	0.377

[a] Stoichiometric amount (mol) of metal cations per mole mineral.
[b] x is fraction of mineral dissolved (1 is assumed totally dissolved, whereas 0.1 means 10% has been dissolved).

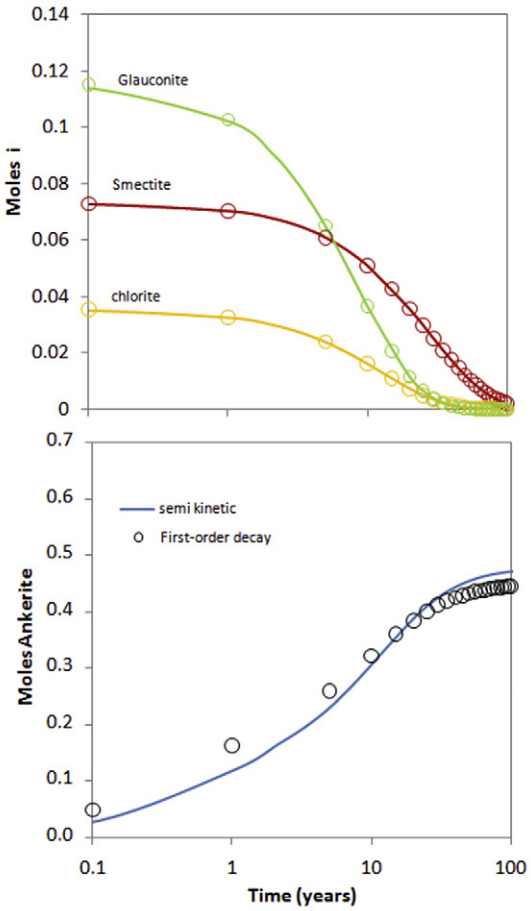

Fig. 8. Comparison of the semi-kinetic approach (Eq. (1)) to hand calculations assuming a first-order decay (Eq. (5)). (a) There is a close match between the semi-kinetic (curves) and the first-order decay (circles) for dissolution rates of glacuonite, smectite, chlorite, and magnetite (not shown here) and (b) comparison of ankerite formation for the two models. The difference between the two models is a consequence of the difference in how pyrite dissolution was solved. For the semi-kinetic, pyrite was a local-equilibrium phase and the amount supplied to the solution varied with time, whereas for the first-order decay model a fixed amount of pyrite was added to the solution at $t = 0$.

6. Recommended procedure for modelling long-term CO_2–water–rock interactions

To successfully model the effect of long-term CO_2–water–rock interactions, we suggest to approach the problem in a stepwise manner, where significant reactions are first identified and the solution methods and simplifications are then decided on based on the complexity of the simulations:

Step 1: *What reactions are significant?* Run 0D batch simulations of your system using a code such as PHREEQCv2 which is easy to use, contains comprehensive thermodynamic databases, and which can incorporate proper kinetic expressions for the minerals. To get the timing and extent of secondary mineral growth right, chose a rate equation for growth, such as Eq. (3) that includes a nucleation rate term. Be aware that the growth rate coefficient is likely orders of magnitude lower than the dissolution rate coefficient. Because data such as initial fractions of reactive minerals and kinetic data commonly are uncertain, run sensitivity tests.

Step 2: How do the fully kinetic simulations compare to natural analogues? The fully kinetic simulations should if possible be compared to data from natural analogues where data such as the length of CO_2 exposure, reaction temperatures, and CO_2 pressures are known (e.g., Gaus et al., 2005b; Jeandel et al., 2010; Pauwels et al., 2007). Such comparisons will normally be qualitative, but they are helpful in constraining the kinetic parameters, which the model is most sensitive on.

Step 3: *How can the reaction calculations be simplified?* After identifying the important reactions, simplifications in the methods (mathematical formulations of the CO_2–water–rock interactions) can be done. How and to what extent the reaction calculations should be simplified is determined by the capability of the numerical tool for the given problem. For small-scale 0D to 2D simulations with simple geometry, it is possible to solve a full set of mineral reactions constrained by kinetic expressions. Such calculations (10,000 years simulations) may take hours for one single batch grid block. If we allow most phases to be at local equilibrium, the run time for such simulations can be reduced down to a few seconds. For basin-scale simulations with complex geometry on the other hand, we can only expect to be able to solve simple equilibrium systems and analytical expressions (see Table 1).

Step 4: *What is the quality of the simplified calculations*? Finally, if your reaction calculations are simplified, compare your final results to the fully kinetic ones. This can be challenging in highly dynamic open real system with variable CO_2 pressures and fluid transport, and requires knowledge on what reactions are significant for a broad range of CO_2 pressures (found during step 1).

7. Summary and conclusions

Successful modelling of mineral reactions and formation water changes induced by CO_2 injection is challenging for several reasons. First, quality thermodynamic and kinetic data for some reactions can be difficult to obtain and it is therefore difficult to choose a set of primary and secondary phases (and possibly intermediate phases) that can fully represent the system; second, no single simple mathematical expression exists that can accurately predict both dissolution and growth rates; and finally, it may cost too much CPU time to solve the full set of geochemical reactions for large-scale reservoir or basin scale simulations.

We showed that when it comes thermodynamic and kinetic data, the largest difficulty is to obtain parameters for mineral nucleation and growth. Growth rate data do exist for secondary carbonates such as dolomite and magnesite, but the onset of growth is still hard to predict as few nucleation rate data exist. We further showed that the common way of modelling mineral growth by extrapolating growth rates from dissolution rate data using transition state theory and the law of mass action may lead to high overpredictions of the growth rates. We have therefore suggested to define separate mathematical expressions for dissolution and growth, and to define a nucleation rate term to generate surface area for the growth of secondary phases.

We finally suggested a stepwise procedure for modelling long-term CO_2–water–rock interactions. The first step in this procedure was to identify the significant geochemical reactions by solving the full system of mineral reactions constrained by kinetic expressions, and further steps were suggested to simplify the system of geochemical reactions to allow reactions to be included in large-scale reservoir or basin-scale simulations.

Acknowledgements

This work has been (partially) funded by SUCCESS centre for CO_2 storage under grant 193825/S60 from Research Council of Norway (RCN). SUCCESS is a consortium with partners from industry and science, hosted by Christian Michelsen Research As.

Appendix A. Supplementary data

Supplementary data associated with this article can be found, in the online version, at http://dx.doi.org/10.1016/j.ijggc.2013.01.027.

References

Aagaard, P., Helgeson, H.C., 1982. Thermodynamic and kinetic constraints on reaction rates among minerals and aqueous solutions: I. Theoretical considerations. American Journal of Science 282 (3), 237–285.

Aagaard, P., Helgeson, H.C., 1983. Activity/composition relations among silicates and aqueous solutions: II. Chemical and thermodynamic consequences of ideal mixing of atoms on homological sites in montmorillonites, illites, and mixed-layer clays. Clays and Clay Minerals 31 (3), 207–217.

Aagaard, P., Egeberg, P.K., Saigal, G.C., Morad, S., Bjorlykke, K., 1990. Diagenetic albitization of detrital K-feldspars in Jurassic, Lower Cretaceous and Tertiary clastic reservoir rocks from offshore Norway; II, Formation water chemistry and kinetic considerations. Journal of Sedimentary Research 60 (4), 575–581.

Aagaard, P., Oelkers, E.H., Schott, J., 2004. Glauconite dissolution kinetics and application to CO_2 storage in the subsurface. Geochimica et Cosmochimica Acta 68 (11), A143–A1143.

Amram, K., Ganor, J., 2005. The combined effect of pH and temperature on smectite dissolution rate under acidic conditions. Geochimica et Cosmochimica Acta 69 (10), 2535–2546.

Arvidson, R.S., Luttge, A., 2010. Mineral dissolution kinetics as a function of distance from equilibrium – new experimental results. Chemical Geology 269 (1–2), 79–88.

Arvidson, R.S., Mackenzie, F.T., 1996. Tentative kinetic model for dolomite precipitation rate and its application to dolomite distribution. Aquatic Geochemistry 2 (3), 273–298.

Arvidson, R.S., Mackenzie, F.T., 1999. The dolomite problem; control of precipitation kinetics by temperature and saturation state. American Journal of Science 299 (4), 257–288.

Béarat, H., et al., 2006. Carbon sequestration via aqueous olivine mineral carbonation: role of passivating layer formation. Environmental Science & Technology 40 (15), 4802–4808.

Bjorlykke, K., Egeberg, P.K., 1993. Quartz cementation in sedimentary basins. AAPG Bulletin 77 (9), 1538–1548.

Brandt, F., Bosbach, D., Krawczyk-Bärsch, E., Arnold, T., Bernhard, G., 2003. Chlorite dissolution in the acid pH-range: a combined microscopic and macroscopic approach. Geochimica et Cosmochimica Acta 67 (8), 1451–1461.

Brantley, S.L., 2008. Kinetics of mineral dissolution. In: Brantley, S.L., Kubicki, J.D., White, A.F. (Eds.), Kinetics of Water–Rock Interactions. Springer Science Business Media, LLC, New York, pp. 151–196.

Brunauer, S., Emmet, P.H., Teller, E., 1938. Adsorption of gases in multimolecular layers. Journal of the American Chemical Society 60, 309–319.

Burton, W.K., Cabrera, N., Frank, F.K., 1951. The growth of crystals and the equilibrium structure of their surfaces. Philosophical Transactions of the Royal Society of London 243, 299–358.

Dove, P.M., Han, N., De Yoreo, J.J., 2005. Mechanisms of classical crystal growth theory explain quartz and silicate dissolution behavior. Proceedings of the National Academy of Sciences of the United States of America 102 (43), 15357–15362.

Gaus, I., Azaroual, M., Czernichowski-Lauriol, I., 2005a. Reactive transport modelling of the impact of CO_2 injection on the clayey cap rock at Sleipner (North Sea). Chemical Geology 217 (3–4), 319–337.

Gaus, I., et al., 2005b. Comparison of long-term geochemical interactions at two natural CO_2-analogues: Montmiral (Southeast Basin, France) and Messokampos (Florina Basin, Greece) case studies. In: Rubin, E.S., et al. (Eds.), Greenhouse Gas Control Technologies, vol. 7. Elsevier Science Ltd., Oxford, pp. 561–569.

Gaus, I., Audigane, P., André, L., Lions, J., Jacquemet, N., Durst, P., Czernichowski-Lauriol, I., Azaroual, M., 2008. Geochemical modelling and solute transport modelling for CO_2 storage, what to expect from it? International Journal of Greenhouse Gas Control 2, 605–625.

Gaus, I., 2010. Role and impact of CO_2–rock interactions during CO_2 storage in sedimentary rocks. International Journal of Greenhouse Gas Control 4, 73–89.

Gautier, J.-M., Oelkers, E.H., Schott, J., 1994. Experimental study of K-feldspar dissolution rates as a function of chemical affinity at 150 °C and pH 9. Geochimica et Cosmochimica Acta 58 (21), 4549–4560.

Golubev, S.V., Bauer, A., Pokrovsky, O.S., 2006. Effect of pH and organic ligands on the kinetics of smectite dissolution at 25 °C. Geochimica et Cosmochimica Acta 70 (17), 4436–4451.

Golubev, S.V., Bénézeth, P., Schott, J., Dandurand, J.L., Castillo, A., 2009. Siderite dissolution kinetics in acidic aqueous solutions from 25 to 100 °C and 0 to 50 atm pCO_2. Chemical Geology 265 (1–2), 13–19.

Gundogan, O., Mackay, E., Todd, A., 2011. Comparison of numerical codes for geochemical modelling of CO_2 storage in target sandstone reservoirs. Chemical Engineering Research and Design 89, 1805–1816.

Helgeson, H.C., 1968. Evaluation of irreversible reactions in geochemical processes involving minerals and aqueous solutions—I. Thermodynamic relations. Geochimica et Cosmochimica Acta 32 (8), 853–877.

Hellevang, H., Declercq, J., Kvamme, B., Aagaard, P., 2010. The dissolution rates of dawsonite at pH 0.9 to 5 and temperatures of 22, 60 and 77 °C. Applied Geochemistry 25 (10), 1575–1586.

Hellevang, H., Declercq, J., Aagaard, P., 2011. Why is dawsonite absent in CO2 charged reservoirs? Oil & Gas Science and Technology - Revue de l'IFP 66 (1), 119–135.

Hellevang, H., Aagaard, P., 2010. On the use of Transition-State-Theory (TST) to predict the potential for carbonate growth in sedimentary basins. GSA, Denver, CO, USA.

Hellmann, R., Daval, D., Tisserand, D., 2010. The dependence of albite feldspar dissolution kinetics on fluid saturation state at acid and basic pH: progress towards a universal relation. Comptes Rendus Geoscience 342 (7–8), 676–684.

Holland, T.J.B., Powell, R., 1998. An internally consistent thermodynamic data set for phases of petrological interest. Journal of Metamorphic Geology 16 (3), 309–343.

Jeandel, E., Battani, A., Sarda, P., 2010. Lessons learned from natural and industrial analogues for storage of carbon dioxide. International Journal of Greenhouse Gas Control 4 (6), 890–909.

Johnson, J.W., Oelkers, E.H., Helgeson, H.C., 1992. SUPCRT92: a software package for calculating the standard molal thermodynamic properties of minerals, gases, aqueous species, and reactions from 1 to 5000 bar and 0 to 1000 °C. Computers & Geosciences 18 (7), 899–947.

Kaszuba, J.P., Viswanathan, H.S., Carey, J.W., 2011. Relative stability and significance of dawsonite and aluminium minerals in geologic carbon sequestration. Geophysical Research Letters 38 (L08404), 1–5.

Knauss, K.G., Johnson, J.W., Steefel, C.I., 2005. Evaluation of the impact of CO_2, co-contaminant gas, aqueous fluid and reservoir rock interactions on the geologic sequestration of CO_2. Chemical Geology 217 (3–4), 339–350.

Lasaga, A.C., 1981. Transition state theory. Reviews in Mineralogy and Geochemistry 8 (1), 135–168.

Lowson, R.T., Comarmond, M.C.J., Rajaratnam, G., Brown, P.L., 2005. The kinetics of the dissolution of chlorite as a function of pH and at 25 °C. Geochimica et Cosmochimica Acta 69 (7), 1687–1699.

Luttge, A., 2005. Etch pit coalescence, surface area, and overall mineral dissolution rates. American Mineralogist 90 (11–12), 1776–1783.

Lüttge, A., 2006. Crystal dissolution kinetics and Gibbs free energy. Journal of Electron Spectroscopy and Related Phenomena 150 (2–3), 248–259.

Marini, L., 2006. Geological sequestration of carbon dioxide thermodynamics, kinetics, and reaction path modeling. In: Reaction Path Modelling of geological CO_2 Sequatration, pp. 319–394 (Chapter 7).

Nagy, K.L., 1995. Dissolution and precipitation kinetics of sheet silicates. In: White, A.F., Brantley, S.L. (Eds.), Chemical Weathering Rates of Silicate Minerals. Mineralogical Society of America, Washington, DC, pp. 173–233.

Oelkers, E.H., Gislason, S.R., 2001. The mechanism, rates and consequences of basaltic glass dissolution: I. An experimental study of the dissolution rates of basaltic glass as a function of aqueous Al, Si and oxalic acid concentration at 25 °C and pH = 3 and 11. Geochimica et Cosmochimica Acta 65 (21), 3671–3681.

Oelkers, E.H., Schott, J., Devidal, J.-L., 1994. The effect of aluminum, pH, and chemical affinity on the rates of aluminosilicate dissolution reactions. Geochimica et Cosmochimica Acta 58 (9), 2011–2024.

Oelkers, E.H., Schott, J., Gauthier, J.-M., Herrero-Roncal, T., 2008. An experimental study of the dissolution mechanism and rates of muscovite. Geochimica et Cosmochimica Acta 72 (20), 4948–4961.

Palandri, J.L., Kharaka, Y.K., 2004. A compilation of rate parameters of water–mineral interaction kinetics for application to geochemical modeling. U.S. Geological Survey Water-Resources Investigations Report 04-1068.

Parkhurst, D.L., Appelo, C.A.J., 1999. User's guide to PHREEQC (version 2) – a computer program for speciation, reaction-path, 1D-transport, and inverse geochemical calculations. U.S. Geological Survey, Water-Resources Investigation Report.

Pauwels, H., Gaus, I., le Nindre, Y.M., Pearce, J., Czernichowski-Lauriol, I., 2007. Chemistry of fluids from a natural analogue for a geological CO_2 storage site (Montmiral, France): lessons for CO_2–water–rock interaction assessment and monitoring. Applied Geochemistry 22 (12), 2817–2833.

Pham, V.T.H., Lu, P., Aagaard, P., Zhu, C., Hellevang, H., 2011. On the potential of CO_2–water–rock interactions for CO_2 storage using a modified kinetic model. International Journal of Greenhouse Gas Control 5, 1002–1015.

Pokrovsky, O.S., Golubev, S.V., Schott, J., 2005. Dissolution kinetics of calcite, dolomite and magnesite at 25 °C and 0 to 50 atm pCO_2. Chemical Geology 217 (3–4), 239–255.

Pokrovsky, O.S., Golubev, S.V., Schott, J., Castillo, A., 2009. Calcite, dolomite and magnesite dissolution kinetics in aqueous solutions at acid to circumneutral pH, 25 to 150 °C and 1 to 55 atm pCO_2: new constraints on CO_2 sequestration in sedimentary basins. Chemical Geology 265 (1–2), 20–32.

Pokrovsky, O.S., Schott, J., 2004. Experimental study of brucite dissolution and precipitation in aqueous solutions: surface speciation and chemical affinity control. Geochimica et Cosmochimica Acta 68 (1), 31–45.

Powell, R., Holland, T., 1999. Relating formulations of the thermodynamics of mineral solid solutions; activity modeling of pyroxenes, amphiboles, and micas. American Mineralogist 84 (1–2), 1–14.

Rimstidt, J.D., Barnes, H.L., 1980. The kinetics of silica–water reactions. Geochimica et Cosmochimica Acta 44 (11), 1683–1699.

Saldi, G.D., Jordan, G., Schott, J., Oelkers, E.H., 2009. Magnesite growth rates as a function of temperature and saturation state. Geochimica et Cosmochimica Acta 73 (19), 5646–5657.

Saldi, G.D., Köhler, S.J., Marty, N., Oelkers, E.H., 2007. Dissolution rates of talc as a function of solution composition, pH and temperature. Geochimica et Cosmochimica Acta 71 (14), 3446–3457.

Saldi, G.D., Schott, J., Pokrovsky, O.S., Oelkers, E.H., 2010. An experimental study of magnesite dissolution rates at neutral to alkaline conditions and 150 and

200 °C as a function of pH, total dissolved carbonate concentration, and chemical affinity. Geochimica et Cosmochimica Acta 74 (22), 6344–6356.
Schott, J., Pokrovsky, O.S., Oelkers, E.H., 2009. The link between mineral dissolution/precipitation kinetics and solution chemistry. Reviews in Mineralogy and Geochemistry 70, 207–258.
Shock, E.L., Helgeson, H.C., 1990. Calculation of the thermodynamic and transport properties of aqueous species at high pressures and temperatures: standard partial molal properties of organic species. Geochimica et Cosmochimica Acta 54 (4), 915–945.
Soave, G., 1972. Equilibrium constants from a modified Redlich–Kwong equation of state. Chemical Engineering Science 27, 1197–1203.
Steefel, C.I., Van Cappellen, P., 1990. A new kinetic approach to modeling water–rock interaction: the role of nucleation, precursors, and Ostwald ripening. Geochimica et Cosmochimica Acta 54 (10), 2657–2677.
Tardy, Y., Duplay, J., 1994. Stability fields of smectites and illites including glauconites as a function of temperature and chemical composition. In: Wolf, K.H., Chilingarian, G.V. (Eds.), Diagenesis IV. Developments in Sedimentology. , pp. 95–132.
Teng, H.H., Dove, P.M., De Yoreo, J.J., 2000. Kinetics of calcite growth: surface processes and relationships to macroscopic rate laws. Geochimica et Cosmochimica Acta 64 (13), 2255–2266.
White, A.F., Brantley, S.L., 2003. The effect of time on the weathering of silicate minerals: why do weathering rates differ in the laboratory and field? Chemical Geology 202 (3–4), 479–506.
White, A.F., Peterson, M.L., Hochella Jr., M.F., 1994. Electrochemistry and dissolution kinetics of magnetite and ilmenite. Geochimica et Cosmochimica Acta 58 (8), 1859–1875.
Xu, T., Apps, J.A., Pruess, K., 2005. Mineral sequestration of carbon dioxide in a sandstone-shale system. Chemical Geology 217 (3–4), 295–318.
Xu, T., Spycher, N., Sonnenthal, E., Zhang, G., Zheng, L., Pruess, K., 2011. TOUGHREACT Version 2: a simulator for subsurface reactive transport under non-isothermal multiphase flow conditions. Computers & Geosciences 37 (6), 763–774.
Yang, L., Steefel, C.I., 2008. Kaolinite dissolution and precipitation kinetics at 22 °C and pH 4. Geochimica et Cosmochimica Acta 72 (1), 99–116.